

Numerical Modelling of Convective Wave using Fractional-Step Method

Wah Yen Tey^{1,2*}, Jared Tang Tze Hou¹, Hooi Siang Kang³

¹Department of Mechanical Engineering, Faculty of Engineering, UCSI University, Kuala Lumpur, Malaysia

²Takasago i-Kohza, Malaysia-Japan International Institute of Technology, Universiti Teknologi Malaysia, Kuala Lumpur, Malaysia

³Faculty of Mechanical Engineering, Universiti Teknologi Malaysia, Skudai, Johor, Malaysia

*Corresponding author Email: teywy@ucsiuniversity.edu.my

Abstract

Wave equation is often solved independently without involving Continuity and momentum equations and this implies that the numerical simulation is restricted to wave phenomenon in static fluid. Meanwhile the available wave models are more suitable for the case in which the convective effect outweighs the local wave fluctuation. However, there are many fluid dynamics phenomena which involves equally significant effect of convective flow and wave disturbance, such as mountain waves, strong aeroacoustics wave and strong ocean waves. These flows need to be simulated by computational coupling. We have developed a solver using fractional step method for the construction of convective wave coupling algorithm. In our implementation, we model a flow across the wave-excited lid driven cavity as our case study, in which the model is to imitate the aerodynamic mountain wave. We found that the convective wave ratio plays a great role in affecting the velocity field of the fluid domain.

Keywords: Computational wave dynamics, Aerodynamic mountain wave, Convective wave, Fractional step method.

1. Introduction

Conventional wave equation is analysed and applied in engineering fields even until today, such as in ultrasonic evaluation [1], magneto-electro-elastic engineering [2] and quantum mechanics [3]. However, such analysis will be confined to a problem domain in which the wave transporting medium only experiences diffusion of scalar variables. Convective wave takes place indeed in many natural phenomenon and engineering applications indeed, such as urban acoustics [4], coastal wave prediction [5], biomedical investigation [6], bubble dynamics [7] and aeroacoustics [8-11]. Therefore, the conventional wave equation is not appropriate for convection wave propagation.

To solve the issue, conventional continuity equation and momentum equations [12] are modified with various ways to fit with the convective nature. Sang [13], Willatzen and Voon [14], Chen et al. [15] and Liu et al. [16] imitated the large eddy simulation (LES) concept to create the vector's fluctuation, producing a "wave-like" domain solved using Fourier theory. Another way of simulating the convective wave is by linearizing the Euler's equations and formulating wave-based models [4]. The examples of such analysis are FVCOM model [15], FVCOM-SWAVE model [17] and convective vector wave analysis [18].

Unfortunately, we found that these available methods are not able to directly represent the convective wave in an explicit manner, as shown in Fig. 1. This is because the perturbation speed refers to the fluid particle speed of fluctuation within a range of distance, while convective speed refers to the fluid particle speed of moving forward [19]. The perturbation speed is not clearly differentiated with the convective speed in the previous numerical schemes.

Moreover, these methods are more suitable for the cases in which the convection speed is much more significant than perturbation

speed. In other words, the available numerical schemes are robust only in solving highly convective wave phenomenon especially the general ocean waves, by obtaining a general wave-influenced flow description for the problem domain. They are not applicable for the phenomena which involve equally dominant convective and wave effect, such as aerodynamic mountain waves, strong aeroacoustics waves and strong ocean waves.

With this regard, we formulated our numerical modelling by coupling the continuity equation, momentums equation and wave equation. Our numerical solver is able to simulate the convective wave for the case in which the perturbation effect is as significant as convection effect.

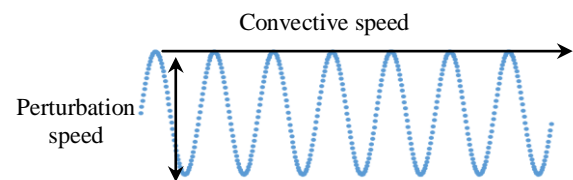


Fig. 1: Perturbation speed and convective speed for wave

2. Physical Modeling

In this paper, we imitate the aviation mountain wave, which is a phenomenon which contains wave fluctuation when the air flows across mountains. Mountain wave could result in atmospheric turbulent and the damage of aircraft [20]. Due to the equally strong convective current and wave undulation, the velocity vector will be altered in both its direction and magnitude, as shown in Fig. 2.

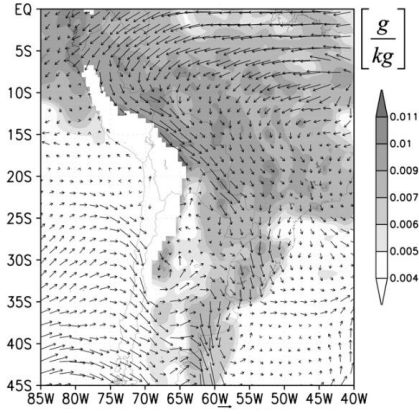


Fig. 2: Velocity vector due to mountain wave near Southern Andes [21]

With this, we take the wave-stimulated lid driven cavity [22] as our case study. The Reynolds number at the top side of the cavity is controlled within laminar region of 5, 50 and 500, while the wave excitation source is located either at the top or bottom part of the cavity. The purpose of low Reynolds number selection is to minimise the difference of velocity vector between the convective velocity and particle perturbation velocity. The physical model can be illustrated as in Fig. 3.

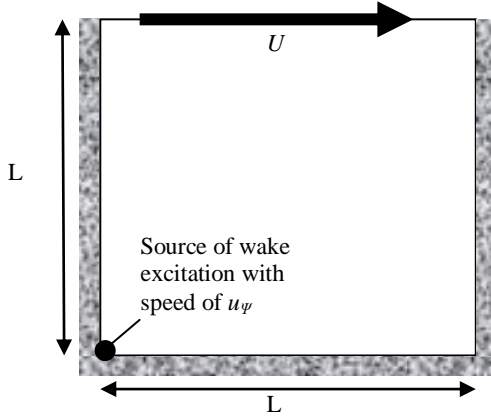


Fig. 3: Physical model for numerical simulation of convective wave in lid driven cavity

We introduce a new parameter of convection-wave ratio which represent the ratio between the strength of convection and wave effect. Mathematically, the convection-wave ratio, ζ is shown as in Equation (1).

$$\zeta = \frac{U}{u_p} \quad (1)$$

where U is the freestream convective velocity while u_p is the fluid particle perturbation speed.

3. Mathematical Modelling of Convective-Wave Coupling Scheme

Our mathematical modelling involves continuity equation, momentum equations and wave equation which can be shown respectively from Equation (2) – (5).

$$\frac{\partial u_x}{\partial x} + \frac{\partial u_y}{\partial y} = 0 \quad (2)$$

$$\frac{\partial u_x}{\partial t} + u_x \frac{\partial u_x}{\partial x} + u_y \frac{\partial u_x}{\partial y} = -\frac{1}{\rho} \frac{\partial P}{\partial x} + \nu \left(\frac{\partial^2 u_x}{\partial x^2} + \frac{\partial^2 u_x}{\partial y^2} \right) \quad (3)$$

$$\frac{\partial u_y}{\partial t} + u_x \frac{\partial u_y}{\partial x} + u_y \frac{\partial u_y}{\partial y} = -\frac{1}{\rho} \frac{\partial P}{\partial y} + \nu \left(\frac{\partial^2 u_y}{\partial x^2} + \frac{\partial^2 u_y}{\partial y^2} \right) \quad (4)$$

$$\frac{\partial^2 u_{\psi}}{\partial t^2} = c^2 \left(\frac{\partial^2 u_{\psi}}{\partial x^2} + \frac{\partial^2 u_{\psi}}{\partial y^2} \right) \quad (5)$$

From Equation (1) – (3), u_x and u_y represents the x - and y - component convective velocity vector respectively, P is the pressure scalar, ρ is the fluid density while ν is the fluid kinematic viscosity. In Equation (4), again, u_{ψ} represents the fluid particle perturbation velocity with c^2 is the ratio between the fluctuation tension and fluid density. In our study, the fluid is regarded as Newtonian fluid

3.1. Fractional Step Method

In our solver, fractional-step method [23] is applied to couple the continuity and momentum equations. The method requires the formation of pressure Poisson equation such that the first derivative of momentum equations is combined with the continuity equation. In fractional step method, the pressure term is temporarily removed from the discretisation. This will form Equation (6) and (7). The superscript $n+1/2$ and n represents the intermediate time step and current time step respectively.

$$(u_x)^{n+1/2} = \Delta t \left\{ u_x - u_x \frac{\partial u_x}{\partial x} - u_y \frac{\partial u_x}{\partial y} + \nu \left(\frac{\partial^2 u_x}{\partial x^2} + \frac{\partial^2 u_x}{\partial y^2} \right) \right\}^n \quad (6)$$

$$(u_y)^{n+1/2} = \Delta t \left\{ u_y - u_x \frac{\partial u_y}{\partial x} - u_y \frac{\partial u_y}{\partial y} + \nu \left(\frac{\partial^2 u_y}{\partial x^2} + \frac{\partial^2 u_y}{\partial y^2} \right) \right\}^n \quad (7)$$

In Equation (6) and (7), the convective terms are discretised via first order upwind scheme while the diffusive terms are discretised via central finite difference scheme, both using finite volume method. With this the intermediate velocity field, $\mathbf{u}^{n+1/2} = \{u_x^{n+1/2}, u_y^{n+1/2}\}$ could be obtained. The intermediate velocity field is then applied into the Poisson equation in order to obtain the pressure field. The Poisson equation is developed by removing the convective and diffusive term from both the momentum equations, taking the first derivative of the respective dimension, and summing them all together. The Poisson equation is demonstrated as in Equation (8).

$$-\frac{1}{\rho} \left(\frac{\partial P^2}{\partial x^2} + \frac{\partial P^2}{\partial y^2} \right)^{n+1} = \frac{\partial}{\partial t} \left(\frac{\partial u_x}{\partial x} + \frac{\partial u_y}{\partial y} \right)^{n+1/2} \quad (8)$$

Note that the Continuity term in Equation (8) shall not diverge due to mass conservation principle. Upon obtaining the pressure field of the next time step, P^n , the momentum equations which negate the convective and diffusive term are revisited to form the velocity field of the next time step.

$$(u_x)_{i,j}^{n+1} = (u_x)_{i,j}^n - \Delta t (P_{i+1,j} - P_{i,j})^{n+1} \quad (9)$$

$$(u_y)_{i,j}^{n+1} = (u_y)_{i,j}^n - \Delta t (P_{i,j+1} - P_{i,j})^{n+1} \quad (10)$$

Several local iterations between Equation (8) – (10) may be needed for convergence, to obtain the velocity, \mathbf{u}^n and pressure, P^n of the next time step. Upon this local convergence, the process will be repeated back to find again the next intermediate velocity field.

The global iterations from Equation (6) – (10) is repeated until convergence, or the required time domain. With this, both the continuity and momentum equations can be satisfied. In our solver, we used staggered grid [24] for the computation.

3.2. Discretisation of Wave Equation

We applied central difference finite volume method to discretise the wave equation. Upon modification, the resulting discretised wave equation can be shown as in Equation (11).

$$(u_\psi)_{i,j}^{n+1} = 2(u_\psi)_{i,j}^n - (u_\psi)_{i,j}^{n-1} - \left(\frac{c\Delta t}{\Delta x}\right)^2 \left\{ 4(u_\psi)_{i,j}^n - (u_\psi)_{nb}^n \right\} \quad (11)$$

The subscript *nb* represents the neighbouring nodes of the node of interest with coordinate of (*i,j*). Note that due to the second order time derivative, the computation of the discretised equation requires the storage of two sets of particle velocity field, which are the current field, u_ψ^n and previous field, u_ψ^{n-1} .

Upon obtaining both the convective speed and perturbation speed, the resultant velocity vector will be in Equation (12).

$$\vec{u} = \sqrt{u_x^2 + u_y^2 + u_\psi^2} \quad (12)$$

3.3. Complete Convective-Wave Coupling Algorithm

The complete convective-wave coupling algorithm is construed by combining Equation (6) – (11), in which the step-by-step methodology can be illustrated in Fig. 4.

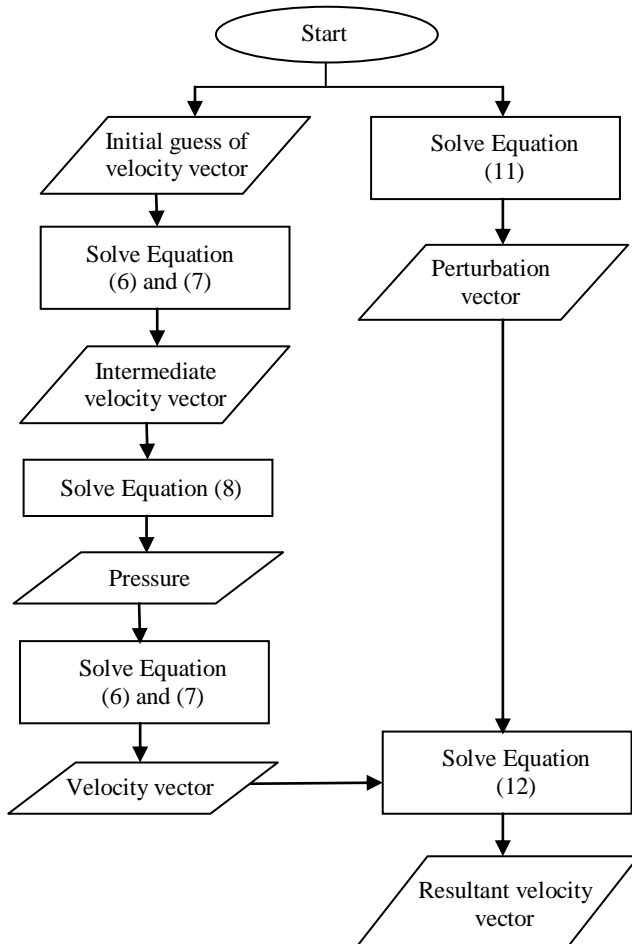


Fig. 4: Perturbation convective-wave coupling algorithm

4. Numerical Analysis

In the implementation of the numerical scheme, the top side of the cavity is set to be Dirichlet boundary condition while the rest of the walls are set as the Neumann boundary condition. The freestream velocity is set as 1 m/s. The Courant number [25] chosen is 0.5 after some trial and error run to reach a balance between the numerical stability and computation effort. The formula of Courant number is shown in Equation (13).

$$\text{Courant number} = \frac{c\Delta t}{\Delta x} \quad (13)$$

The grid size applied is 32×32 . Since the wave is naturally unsteady, we do not set a global convergence criterion to stop the time-stepping coupling. The simulation can be executed to any prescribed time-stepping according to the requirement of the time of result observation. In our work, we set to have 1000 iterations of time stepping for result computation. The source of wave excitation is located at the top left and bottom left of the cavity.

4.1. Effect of Location of Wave Excitation

When the wave excitation is located at the bottom left of the cavity, the velocity vector is altered the most from the bottom left too, with attenuating effect passing to the top-right. Meanwhile if the wave excitation is located at the top left of the cavity, the velocity of the flow recirculation region will have some undulation. These can be shown at Fig. 5 and Fig. 6. The value of convection-wave ratio set is 1, which implies the equivalent effect between the convection and wave fluctuation.

Fig. 5(a) – 5(c) illustrated the effect of the wave excitation from the bottom left of the cavity to the velocity vector at different Reynolds number, *Re*, which can be defined in Equation (14).

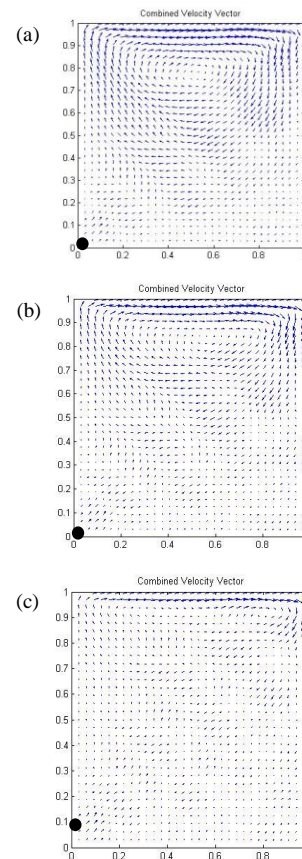


Fig. 5: Velocity vector when the source of wave excitation is located at the bottom left for the case of (a) *Re* = 5; (b) *Re* = 50; (c) *Re* = 500

$$Re = \frac{\rho UL}{\mu} \quad (14)$$

μ is the dynamic viscosity of the fluid. Meanwhile from Fig. 6(a) – (c), the location of source of wave excitation is located at the top left of the cavity.

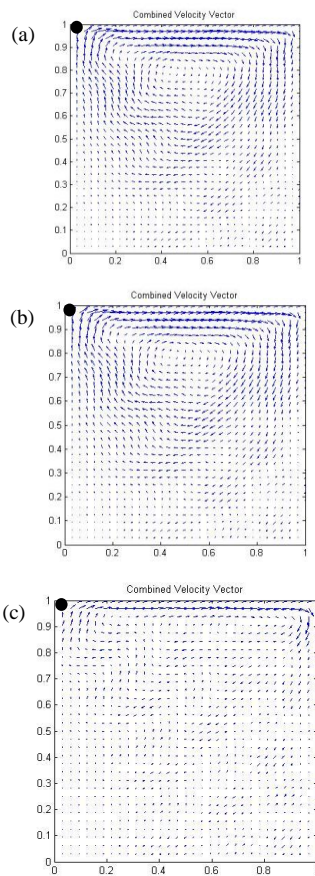


Fig. 6: Velocity vector when the source of wave excitation is located at the top left for the case of (a) $Re = 5$; (b) $Re = 50$; (c) $Re = 500$

Generally, the flow pattern follows the convective lid driven cavity flow, with just a difference in the resultant velocity vector due to the wave disturbance. In some of the region, especially at the low Reynolds number, the alternating high-low velocity amplification across the dimension is so apparent.

4.2. Effect of Convection-Wave Ratio

To observe the fluid dynamic effect due to different convection-wave ratio, we fix the wave excitation source at the bottom of the cavity while the Re as 5. From our investigation, the resultant velocity fluctuation is the strongest at low convection-wave ratio. The results can be demonstrated from Fig. 7(a) – (c).

4.3. Numerical Convergence on Continuity Requirement

The numerical convergence of our solver is also tested. At higher Re , the error overshoot is smaller yet with a slower convergence speed. This may due to the larger pressure fluctuation inside the cavity which may drag the time for the scheme to converge. While at lower Re , the error overshoot is much larger but with a faster convergence speed. These can be revealed as from Fig. 8(a) – (c). The convergence studies shown here refer to the case at convection-wave ratio of 1.4. The Continuity convergence requirement is set as 1×10^{-4} .

In general, the results converge and this implies that our solver is numerically consistent and stable [26]. Since the fractional step

method is applied, the under-relaxation index as used in SIMPLE algorithm is not required.

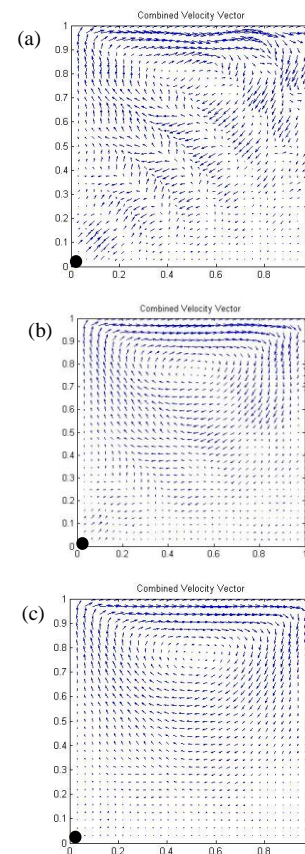


Fig. 7: Velocity vector when the source of wave excitation is located at the bottom left at $Re = 5$ for the case of (a) $\zeta = 0.8$; (b) $\zeta = 1.0$; (c) $\zeta = 1.4$

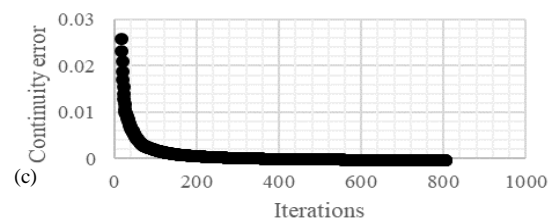
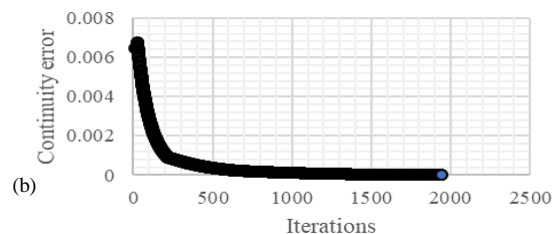
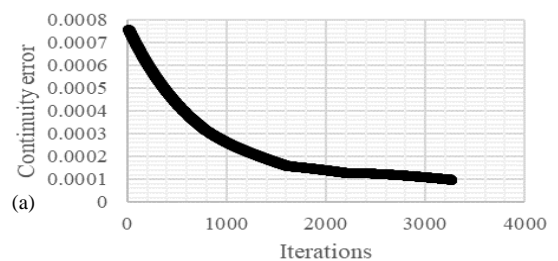


Fig. 8: Convergence study for the case of $\zeta = 1.4$ at (a) $Re = 5$; (b) $Re = 50$; (c) $Re = 500$

5. Conclusion

In conclusion, convective wave coupling numerical scheme has been developed using fractional step method. The convergence of the scheme has been proven, and it is applicable for numerical modelling when the convection wave ratio is small. The smaller the convection wave ratio, the higher alternating high-low velocity amplification.

Acknowledgement

This research is supported by Pioneer Scientist Incentive Fund (PSIF) with grant number Proj-In-FETBE-038, Centre of Excellence for Research, Value Innovation and Entrepreneurship (CERVIE), UCSI University Kuala Lumpur, Malaysia.

References

- [1] Hernandez V, Estrada J, Moreno E, Rodríguez S & Mansur A, "Numerical solution of a wave propagation problem along plate structure based on the isogeometric approach", *Journal of Theoretical and Computational Acoustics*, Vol.26, No.1, (2018), pp.1750030.
- [2] Seadawy AR & Manafian J, "New soliton solution to the longitudinal wave equation in a magneto-electro-elastic circular rod", *Results in Physics*, Vol.8, (2018), pp.1158-1167.
- [3] Tan CZ, "Wave equation for energy and the momentum of a moving particle", *Optik*, Vol.168, (2018), pp.864-872.
- [4] Hornikx M, "Ten questions concerning computational urban acoustics", *Building and Environment*, Vol.106, (2016), pp.409-421.
- [5] Venugopal V, Nimaladinne R & Vogler A, "Numerical modelling of wave energy sources and assessment of wave energy extraction by large scale wave farms", *Ocean and Coastal Management*, Vol.147, (2017), pp.37-48.
- [6] Ma X, Huang B, Wang G, Fu X & Qiu S, "Numerical simulation of the red blood cell aggregation and deformation behaviours in ultrasonic field", *Ultrasonic Sonochemistry*, Vol.38, (2017), pp.604-613.
- [7] Liu J, Wang W, Chu N, Wu D & Wu W, "Numerical simulations and experimental validation on passive acoustics emissions during bubble formation", *Applied Acoustics*, Vol.130, (2018), pp.34-42.
- [8] Astley RJ & Gamallo P, "Special shortwave elements for flow acoustics", *Computer Methods in Applied Mechanics and Engineering*, Vol.194, (2015), pp.341-353.
- [9] Barbarino M, Adamo FP, Bianco D, & Bartoccini D, "Hybrid BEM/empirical approach for scattering of correlated sources in rocket noise prediction", *Journal of Sound and Vibration*, Vol.403, (2017), pp.90-103.
- [10] Adam, AR & Chaudhari MB, "Acoustic Study and behaviour of flow through orifice", *Procedia Manufacturing*, Vol.20, (2018), pp.154-159.
- [11] Chirico G, Barakos GN & Bown N, "Propeller installation effects on turboprop aircraft acoustics", *Journal of Sound and Vibration*, Vol.424, (2018), pp.238-262.
- [12] Tey WY, Asako Y, Sidik NAC & Goh RZ, "Governing equations in computational fluid dynamics: derivations and a recent review", *Progress in Energy and Environment*, Vol.1, (2017), pp.1-19.
- [13] Sang JG, "On the dynamics of convection waves", *Quarterly Journal of the Royal Meteorological Society*, Vol.119, (1993), pp.715-732.
- [14] Willatzen M & Voon LCLY, "Flow acoustics in periodic structure", *Ultrasonics*, Vol.43, (2005) pp.756-763.
- [15] Chen C, Liu H & Beardsley RC, "An unstructured grid, finite-volume, three-dimensional, primitive equation ocean model: application to coastal ocean and estuaries", *Journal of Atmospheric and Oceanic Technology*, Vol.20, (2003), pp.159-186.
- [16] Liu J, Wang W, Chu N, Wu D & Wu W, "Numerical simulations and experimental validation on passive acoustics emissions during bubble formation", *Applied Acoustics*, Vol.130, (2018), pp.34-42.
- [17] Qi J., Chen C, Beardsley RC, Perrie W, Cowles GW & Lai Z, "An unstructured-grid finite-volume surface wave model (FVCOM-SWAVE): implementation, validations and applications", *Ocean Model*, Vol.28, (2009), pp.153-166.
- [18] Mao Y & Hu Z, "Convective wave equation of aeroacoustics", *Procedia IUTAM*, Vol.20, (2017), pp.81-88.
- [19] Ver IL & Beranek, LL, *Noise and Vibration Control Engineering: Principle and Applications*, John Wiley & Sons, Inc, (2006).
- [20] Feltz WF, Bedka KM, Otkin JA, Greenwald T, Ackerman SA, "Understanding satellite-observed mountain wave signatures using high resolution numerical model data", *Weather and Forecasting*, Vol.24, (2009), pp.76-86.
- [21] Torre Adl, Hierro R, Llamado P, Rolla, A & Alexander P, "Severe hailstorms near Southern Andes in the presence of mountain waves", *Atmospheric Research*, Vol.101, (2011), pp.112-123.
- [22] Lee CN, Tey WY & Tan LK, "The Investigation of SIMPLE and SIMPLER algorithm through lid driven cavity", *Journal of Advanced Research in Fluid Mechanics and Thermal Sciences*, Vol.29, (2017), pp.10-23.
- [23] Kajishima T & Taira K, *Computational Fluid Dynamics: Incompressible Turbulent Flows*, Springer International Publishing, (2017).
- [24] Harlow FH & Welch J.E, "Numerical Calculation of Time-Dependent Viscous Incompressible Flow of Fluid with Free Surface", *Physics of Fluid*, Vol.8, (1965), pp.2182-2189.
- [25] Ferziger JH & Peric M, *Computational Methods for Fluid Dynamics*, Springer International Publishing, (2002).
- [26] Tu J, Yeoh GH & Liu C, *Computational Fluid Dynamics: A Practical Approach*, Elsevier Publisher, (2018), pp.117-216.